

This article appeared in a journal published by Elsevier. The attached copy is furnished to the author for internal non-commercial research and education use, including for instruction at the authors institution and sharing with colleagues.

Other uses, including reproduction and distribution, or selling or licensing copies, or posting to personal, institutional or third party websites are prohibited.

In most cases authors are permitted to post their version of the article (e.g. in Word or Tex form) to their personal website or institutional repository. Authors requiring further information regarding Elsevier's archiving and manuscript policies are encouraged to visit:

<http://www.elsevier.com/copyright>



Contents lists available at SciVerse ScienceDirect

Computational and Theoretical Chemistry

journal homepage: www.elsevier.com/locate/comptc

A model system with intramolecular hydrogen bonding: Effect of external electric field on the tautomeric conversion and electronic structures

Venelin Enchev^{*}, Valentin Monev, Nadezhda Markova, Marin Rogozherov, Silvia Angelova, Milena Spassova

Institute of Organic Chemistry, Bulgarian Academy of Sciences, 1113 Sofia, Bulgaria

ARTICLE INFO

Article history:

Received 14 July 2012

Received in revised form 22 November 2012

Accepted 24 November 2012

Available online 7 December 2012

Keywords:

Tautomerism

Electric field

GAPT

Ab initio

ABSTRACT

A new model tautomeric system with intramolecular hydrogen bonding is proposed. Geometry optimizations are performed at HF and MP2 levels and absorption spectra are simulated at TDDFT level. The MP2 level of theory was chosen for studying the effect of the external electric static field (EF) on the molecular electronic structure. The geometries of the tautomers as well as the transition states are fully optimized for each magnitude and for opposite directions of the applied EF. Upon variation of the electric field strength and polarity, it is possible to stabilize different tautomeric forms of the molecule. The dipole moment, HOMO–LUMO gap and the spatial distribution of the frontier orbitals are found to be sensitive to the EF strength and polarity and the different tautomeric structures are differently affected by the field. Elongation of the conjugated system providing a large number of possible tautomeric forms is also examined at HF level. Systems similar to the studied model system have potential use in the design of new molecular electronic devices.

© 2012 Elsevier B.V. All rights reserved.

1. Introduction

The idea of using organic molecules as functional units in electronic devices has received great attention. The assumption of Aviram and Ratner [1] that a single organic molecule could perform as a molecular rectifier may be regarded as the beginning of molecular electronics. A wide variety of molecules have been suggested as molecular devices, such as molecular wires [2–4], molecular diodes [5,6], molecular storage devices [7,8], molecular switches [9–11] and molecular logic gates [12]. Among the various kinds of molecules that can act as molecular devices, conjugated organic molecules favor electron transport of charge carriers along the chain. Due to the delocalization of π -electrons along the chain backbone, particular electrical and optical properties (large non-linear optical responses) arise [13]. It is found that molecules having quinoid structure or molecules which acquire such a pattern after structural changes provoked by external factors like light, electrical field (EF) possess a high degree of electron delocalization, planarity and small energy gap [14]. These properties of such molecules can be used to design bridge units between donor–acceptor fragments of molecular wires. The presence or the rise of extended π -electronic conjugation of bridge units promote strong coupling between donor–acceptor fragments. Many theoretical studies are

devoted to the design of molecular devices by adopting first-principle studies of the effect of an applied external EF on their molecular properties such as electron transfer in conjugated molecular wires [15–19] and conformational dependencies [20,21], and they confirm that the above mentioned properties of bridge units favor a high conductivity in molecular wires.

Another concept for the achievement of the required molecular performance can be realized by tautomeric conversion via fast proton transfer reaction between keto and enol tautomeric forms, each of them with distinct molecular properties. An important feature in such a reaction mechanism is the coupling between the proton motion and the electron density redistribution known as Proton Coupled Electron Transfer (PCET) [22]. The application of EF in a specific direction may favor the proton transfer so as to obtain a tautomer with desired properties. Studies on tautomeric systems in EF are scarce [23–25].

In some cases the tautomeric forms are near in energy and the tautomerization barriers are low enough. Then the application of an external EF with an appropriate magnitude and direction could change the tautomeric equilibrium in the desired direction, that is, EF could be used as a tool to yield a tautomer with desired properties.

We propose a new model system with a possible keto–enol tautomerism. The structure consists of three different fragments – benzoxazolyl (**Bo**), hydroxypyridil (**Hp**) and indanedionyl (**Ind**) where **Hp** is regarded as a bridge (Fig. 1). The presence of different bridge units **Hp** ($n = 1–3$, Fig. 1) leads to a large number of possible

^{*} Corresponding author. Fax: +359 2 8700225.

E-mail address: venelin@orgchm.bas.bg (V. Enchev).

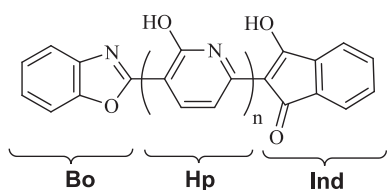


Fig. 1. Structural formula of compounds **1** ($n = 1$), **2** ($n = 2$) and **3** ($n = 3$).

tautomeric forms as well as to a large number of possible tautomeric conversions between them. Detailed study of the EF effect on the electronic and geometric structure of compound **1** ($n = 1$, Fig. 1) is performed for understanding its molecular electrical properties.

2. Computational details

The geometries of the possible tautomers of 2-(5-(benzo[d]oxazol-2-yl)-6-hydroxypyridin-2-yl)-3-hydroxy-1H-inden-1-one (**1**)

(Fig. 2) were located at HF and MP2 levels of theory with Pople's 6-31G(d,p) basis set using the quantum chemistry package, Firefly, version 7.1.H [26]. To investigate the chain length effect, 2-(5-(benzo[d]oxazol-2-yl)-2',6'-dihydroxy-2',3'-dihydro-[2,3'-bipyridin]-6'(1'H)-ylidene)-1H-indene-1,3(2H)-dione (**2**) and 2-(5-(benzo[d]oxazol-2-yl)-2',2'',6'-trihydroxy-[2,3':6',3''-terpyridin]-6''(1''H)-ylidene)-1H-indene-1,3(2H)-dione (**3**) (see Fig. 1, $n = 2, 3$), were considered. Because of the size of the molecules, the calculations were performed at HF/6-31G(d,p) level. Li et al [27] have performed comprehensive tests at the HF level on the typical molecular wire, polyacetylene with a wide variety of basis sets, showing that HF/6-31G(d) is relatively "good", and can be used with sufficient accuracy and sustainable computing time.

Full geometry optimizations of the structures investigated were performed without symmetry constraints. The local minima and transition states were verified by establishing that the Hessians had zero and one negative eigenvalues, respectively. Starting from the transition state, the reaction path was generated as the steepest descent path in mass-scaled coordinates (intrinsic reaction coordinate, IRC) using the Gonzalez–Schlegel algorithm, employing

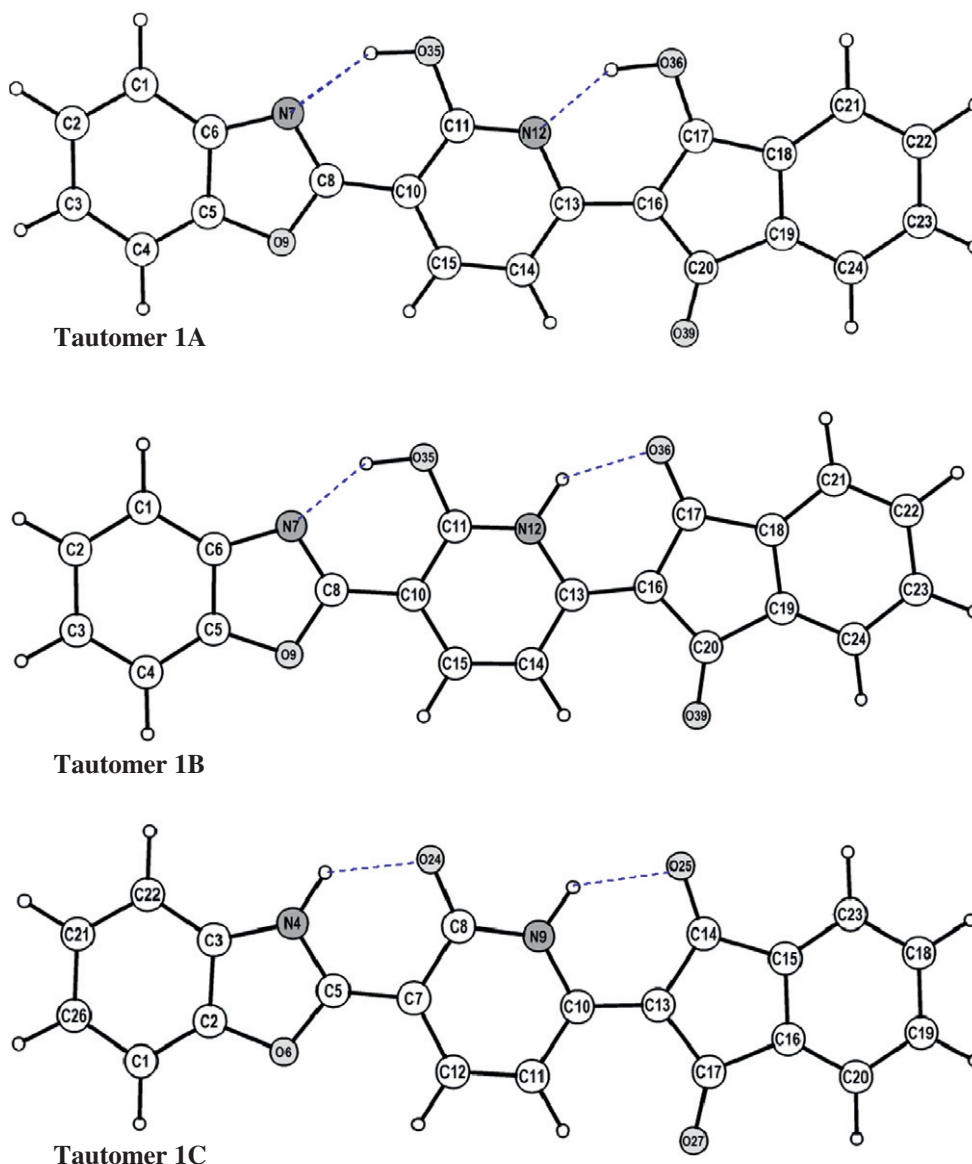


Fig. 2. MP2/6-31G(d,p) optimized structures of tautomers **1A–1C** with numbering of the atoms.

a step size of 0.05 Bohr (1 Bohr corresponds to 0.53 Å). On both branches of the reaction coordinate 30 steps were performed. The values of Gibbs free energies (ΔG) and activation barriers (ΔG^\ddagger) were calculated for a temperature of 298.15 K.

Prior to the introduction of electric field (EF), structures **1A**, **1B** and **1C** (Fig. 2) and their respective transition states were optimized at MP2/6-31G(d,p) level. Electric field effects on the structural and electronic properties of the proposed molecule were studied by analyzing molecular electronic parameters by including a field term in the Hamiltonian of the molecule during geometry optimization. The EF strength is given in atomic units (a.u.) within the numerical range -0.01 to 0.01 a.u. with an increment of 0.001 a.u.

Generalized Atomic Polar Tensors (GAPTs) charges [28] were calculated via numerical derivative procedures implemented in Firefly involving finite-field differencing of the molecular gradient. This requires seven energy + gradient calculations to get the entire dipole derivative matrix. The calculations can be performed at any molecular geometry. For achieving convergence of the dipole moment derivatives, electric field amplitude of 0.0001 a.u. was used, and the overall precision of the calculations was extra high.

Excitation energies were obtained from time-dependent DFT (TDDFT) calculations at the MP2 optimized ground state geometries (vertical excitation) using the hybrid Exchange–Correlation (XC) functionals, B3LYP and PBE0, and the 6-31+G(d,p) basis set. B3LYP has been applied for determination of the excitation energies of a broad range of organic compounds [29–33]. The choice of PBE0 is based on the statement that it is reliable in the evaluation of vertical excitation energies [34–37]. The spectra were simulated by associating to each transition a 50/50 Gaussian/Lorentzian line shape having a height proportional to the oscillator strength and a full width at half-maximum (fwhm) of 0.1 eV. The TDDFT calculations were done using the Gaussian 09 suite of programs [38].

3. Results and discussion

3.1. Tautomeric conversions

We start our discussion considering the values of the energy differences between the tautomers of compound **1** calculated at HF/6-

31G(d,p) and MP2/6-31G(d,p) levels of theory (Table 1). At HF level the most stable is tautomer **1C** followed by tautomers **1B** and **1A**, and the energy differences are very close in gas phase at 0 K (ΔH_0) and at room temperature (ΔG_{298}). Surprisingly, HF calculations predict the quinoid tautomer **1C** as most stable. At MP2 level when only total energy (E_t) is considered, the most stable tautomer becomes **1B**. Tautomer **1A** is next in energy by only 0.90 kcal mol $^{-1}$ and **1C** is higher in energy. The results are similar when the zero-point energy (ZPE) is added to the total energies. The values of the relative free energies (ΔG_{298}) suggest that the most stable tautomer is **1A** followed by **1B** (1.05 kcal mol $^{-1}$) and **1C** (5.03 kcal mol $^{-1}$). The MP2 calculated N7...O35 distances in the tautomers of the compound are 2.685 , 2.642 and 2.599 Å for **1A**, **1B** and **1C**, respectively, and the N12...O36 distances – 2.634 , 2.679 and 2.738 Å for **1A**, **1B** and **1C**, respectively (Fig. 2). They are near to typical values for strong O–H...N and O...H–N intramolecular hydrogen bonds.

The transition state structures corresponding to the intramolecular proton transfer reactions were located (Fig. 3a). According to the calculated values of the proton transfer barriers between the tautomers of compound **1**, two consecutive proton transfer reactions should be considered. At HF level, the free energy barriers of the reactions **1C** \rightarrow **1B** and **1B** \rightarrow **1A** are 9.31 and 7.72 kcal mol $^{-1}$, respectively (Fig. 3a and Table 1). However, the MP2/6-31G(d,p) calculations show that the two tautomerization reactions in reverse direction should occur, i.e. **1A** \rightarrow **1B** and **1B** \rightarrow **1C** (Table 1). The value of the **1A** \rightarrow **1B** reaction barrier is lower than that for **1B** \rightarrow **1C**. The activation energy of the tautomerization reactions via direct intramolecular proton transfer is low enough and the tautomerization process should occur. Hence, according to our calculations, when the electron correlation at MP2 level is taken into account, the consecutive tautomeric conversions **1A** \rightarrow **1B** \rightarrow **1C** take place.

We consider the effect of chain lengthening by adding one ($n = 2$) and two ($n = 3$) hydroxypyridine rings between the indandione and benzoxazole moieties. In the case of $n = 2$, eight tautomeric structures are possible. When two hydroxypyridil rings are added ($n = 3$), the number of possible tautomers increases to sixteen. Because of the size of these molecules, the calculations were performed at HF/6-31G(d,p) level. Here we consider only the energy preferred tautomers of compounds **2** and **3**. All the tautomeric structures of **2** and **3**, and the energy differences between them are presented in Supplementary material (Figs. S1, S2 and Table S1).

The total energies of the tautomers of **2** reveal that at HF level the most stable structure **2A** is followed by **2B** (1.39 kcal mol $^{-1}$) and **2C** (1.43 kcal mol $^{-1}$) (Table 1). There is a small increase in the enthalpy differences (ΔH_0) between tautomers **2A** and **2B** and a decrease in ΔH_0 between **2A** and **2C**. The values of the relative free energies ΔG_{298} of the tautomers of **2** presented in Table 1 show a very small variation. Since the results for ΔG_{298} show the same trend as in the case for ΔH_0 , the stability sequence according to ΔG_{298} values is **2A** \rightarrow **2C** \rightarrow **2B**.

In the case of **3**, 16 tautomers are possible (Fig. S2) and the geometry optimization was carried out at HF/6-31G(d,p) level. The results suggest (Table 1) there are several low-energy tautomers whose total energies are nearly degenerate. **3A** is the most stable, but it is only 0.10 kcal mol $^{-1}$ below **3B**. The energy differences between **3A** and the next stable tautomers, **3C** and **3D** are small – 1.61 and 1.75 kcal mol $^{-1}$. The pattern becomes different when the $T\Delta S$ term is taken into consideration. The most stable structure of **3** becomes **3B**, followed by **3A** (0.87 kcal mol $^{-1}$), **3C** (2.33 kcal mol $^{-1}$) and **3D** (2.77 kcal mol $^{-1}$). As can be seen, the influence of the $T\Delta S$ term is more expressed in the case of compound **3** than **2** and this leads to a rearrangement of the relative free energy sequence.

Table 1
HF/6-31G(d,p) and MP2/6-31G(d,p) calculated energy differences and barriers (kcal mol $^{-1}$), and imaginary frequencies, ν^\ddagger (cm $^{-1}$), for the tautomers of compounds **1–3**.

Compound	HF/6-31G(d,p)				MP2/6-31G(d,p)			
	ΔE_t	ΔH_0	ΔG_{298}	ν^\ddagger	ΔE_t	ΔH_0	ΔG_{298}	ν^\ddagger
1A	3.33	3.51	3.55		0.90	0.24	0.00	
1B	0.26	0.53	0.62		0.00	0.00	1.05	
1C	0.00	0.00	0.00		4.54	4.26	5.13	
TS1 (1A \rightarrow 1B)	10.82	7.88	8.34	1732i	4.57	1.71	3.05	1233i
TS2 (1B \rightarrow 1C)	11.86	8.86	9.31	1702i	6.85	4.21	5.57	1065i
2A	0.00	0.00	0.00					
2B	1.39	1.43	1.53					
2C	1.43	1.29	1.25					
TS1 (2A \rightarrow 2B)	7.55	4.44	4.97	1594i				
TS2 (2B \rightarrow 2C)	12.11	8.99	9.42	1700i				
3A	0.00	0.00	0.87					
3B	0.10	0.05	0.00					
3C	1.61	1.56	2.33					
3D	1.75	1.82	2.77					
TS1(3A \rightarrow 3B)	6.94	3.77	4.89	1607i				
TS2(3B \rightarrow 3C)	7.63	4.55	5.93	1584i				
TS3(3C \rightarrow 3D)	12.34	9.27	10.55	1698i				

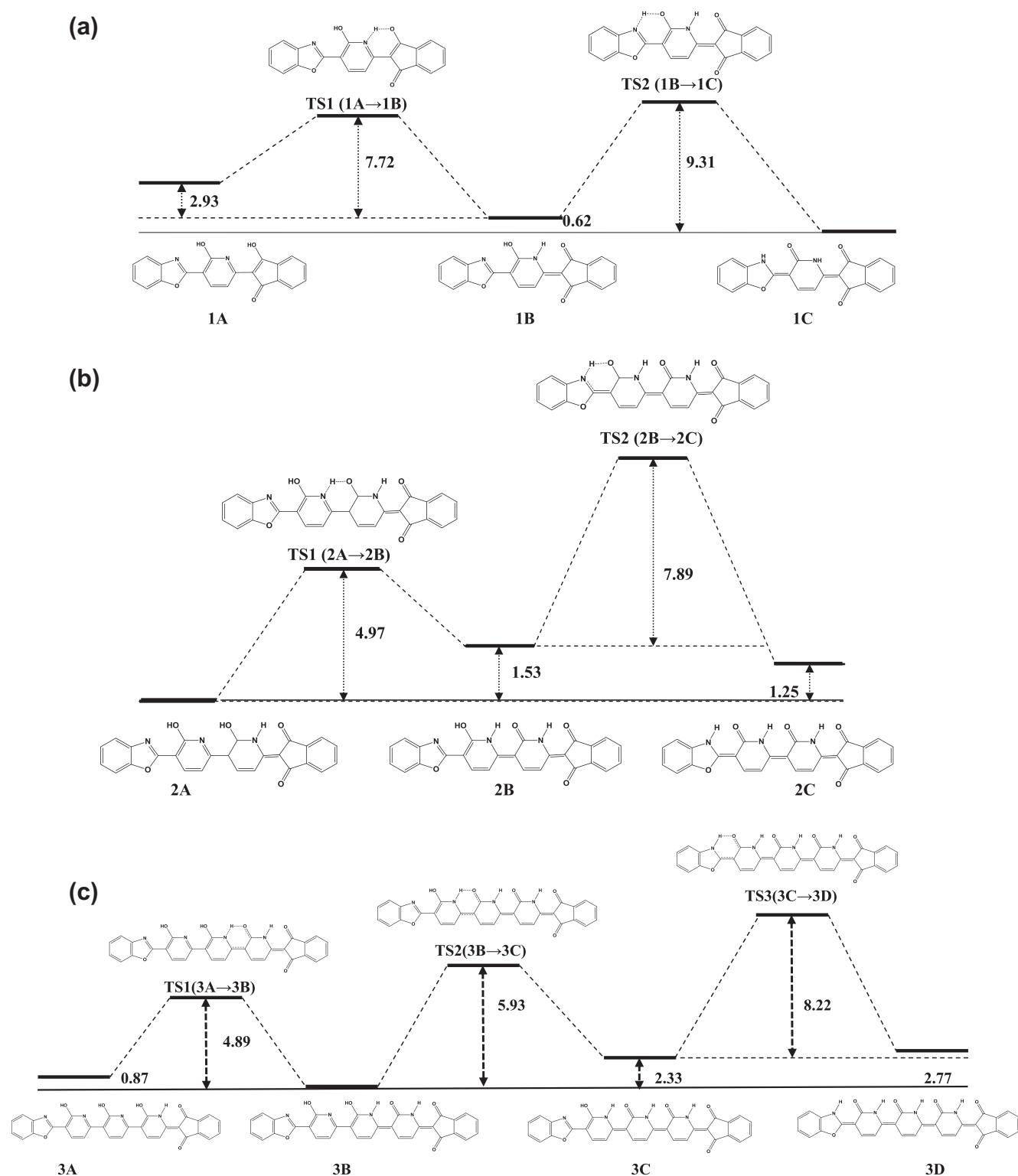


Fig. 3. Tautomeric conversions in compounds **1** (a), **2** (b) and **3** (c). HF/6-31G(d,p) calculated relative energies (ΔG_{298}) and energy barriers (ΔG_{298}^\ddagger) are in kcal mol⁻¹.

In this study we consider the possibility of consecutive conversion of the tautomers of **2** and of **3** by prototropic tautomeric rearrangement. The TS structures corresponding to the proton transfer reactions were localized. The predicted TS's were verified by establishing that the Hessians each had only one negative eigenvalue.

The calculated barriers of tautomerization of **2** and of **3** and the respective imaginary frequencies, calculated at HF/6-31G(d,p) level of theory, are presented in Table 1.

The conversion of **2A** to **2C** is realized by two consecutive tautomeric reactions **2A** → **2B** and **2B** → **2C**. Reaction **2A** → **2B** has a

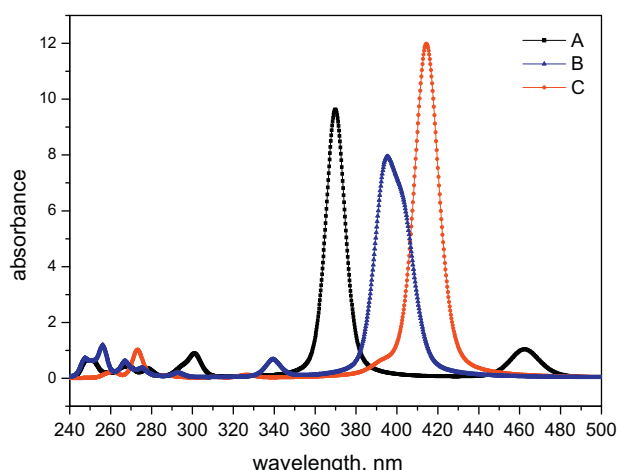


Fig. 4. B3LYP/6-31+G(d,p) calculated UV-vis spectra of tautomers **1A–1C**. The structures are optimized at MP2/6-31G(d,p) level.

lower barrier ($4.97 \text{ kcal mol}^{-1}$) than **2B** \rightarrow **2C** ($7.89 \text{ kcal mol}^{-1}$) but the free energy difference between **2A** and **2B** ($1.53 \text{ kcal mol}^{-1}$) is larger than between **2B** and **2C** ($0.26 \text{ kcal mol}^{-1}$) (Fig. 3b) and reaction **2B** \rightarrow **2C** is exothermic.

The tautomeric conversion of **3** is slightly different from that of **2**. The most stable structure is **3B** and the tautomeric conversion proceeds by two consecutive tautomeric reactions **3B** \rightarrow **3C** and **3C** \rightarrow **3D**. Reaction **3B** \rightarrow **3A** is characterized by the lowest barrier height ($4.89 \text{ kcal mol}^{-1}$). The free energy barriers of the **3B** \rightarrow **3C** and **3C** \rightarrow **3D** reactions amount to $5.93 \text{ kcal mol}^{-1}$ and $8.22 \text{ kcal mol}^{-1}$, respectively (Fig. 3c).

Because of the comparatively low activation barriers and small free energy differences, the tautomeric conversions in compounds **2** and **3** should occur.

3.2. Absorption spectra of the tautomers of compound **1**

The theoretical prediction of the main characteristics of optical absorption is useful for elucidating the electronic structure, and the simulation of these spectra could, in principle, help the experimental recognition of the different structures. For lack of experimental

data the performance of the different theoretical models cannot be assessed. The theoretical considerations and spectra simulations were carried out at TDDFT level using the B3LYP and PBE0 functionals. The B3LYP predicted excitation wavelengths of the tautomers are systematically red shifted with respect to PBE0 but by less than 15 nm and the ordering and relative positions of the transitions for the three tautomers predicted by both functionals is the same. Since the simulated spectra with the two functionals are very similar, we present here only the B3LYP results (Fig. 4). The PBE0 simulated spectra and their comparison to the B3LYP spectra are given in Supp. data section (Figs. S3 and S4).

The simulated absorption spectra of the three tautomers are quite distinct. In the range 320–500 nm **1A** and **1B** have two transitions while **1C** is characterized by only one (Fig. 4). For all systems the HOMO's are delocalized all over the molecule. The LUMO's of **1B** and **1C** are also spread over the whole system whereas **1A**'s LUMO is partially localized on the **Hp** and **Ind** fragments. Due to the pronounced charge transfer (CT) character of $S_0 \rightarrow S_1$, the transition at 462 nm (predominantly contributed by HOMO \rightarrow LUMO) of **1A** is red shifted relative to the respective transitions of **1B** and **1C**. There are two transitions $S_0 \rightarrow S_1$ (404 nm) and $S_0 \rightarrow S_2$ (394 nm) in **1B** with comparable oscillator strengths and contributions from HOMO \rightarrow LUMO and HOMO \rightarrow LUMO + 1 transitions. As in the case of **1A**, there are also contributions from CT states built from the LUMO + 1 orbital localized on fragment **Ind** (Fig. 5). The long wavelength band of **1C** consists of only one pure HOMO \rightarrow LUMO transition (414 nm) with high oscillator strength.

3.3. Electric field dependence

We performed theoretical investigations on the applied external EF effect on the molecular geometry and electronic structure of the tautomers of the title compound. We adopted the following model to account for the external static EF: the molecules are placed in a homogeneous external electric field so that its direction coincides with the x -axis of the standard molecular orientation without a field applied. The field is set as “positive” when the direction is from the benzoxazole to the indandione fragment and as “negative” in the opposite direction.

The Gibbs free energy differences between the tautomers change depending on the EF direction as presented on Fig. 6. In positive external EFs, the effect is confined to a polarization of

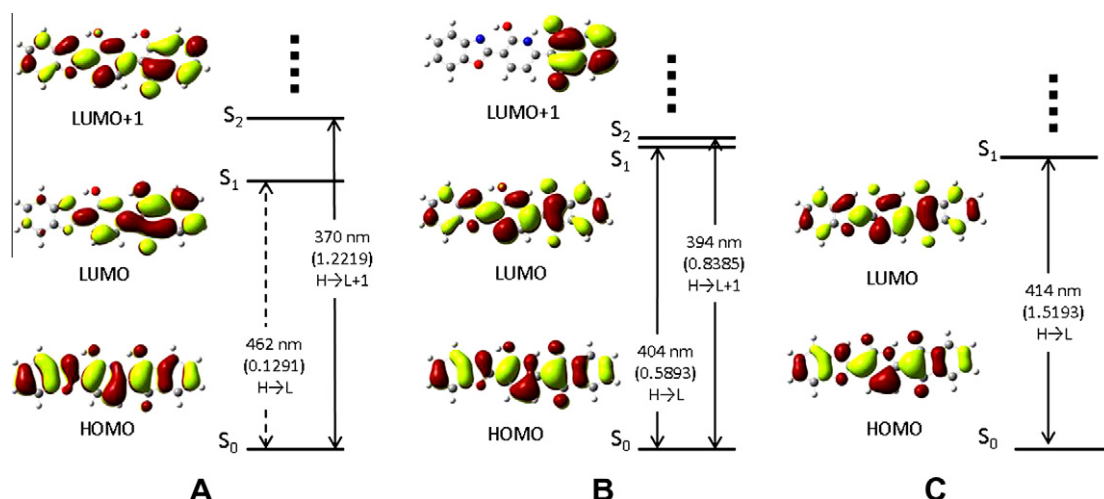


Fig. 5. Graphical representation of the $S_0 \rightarrow S_1$ and $S_0 \rightarrow S_2$ electronic transitions and frontier molecular orbitals of all tautomers of **1**. The calculated oscillator strengths are given in brackets.

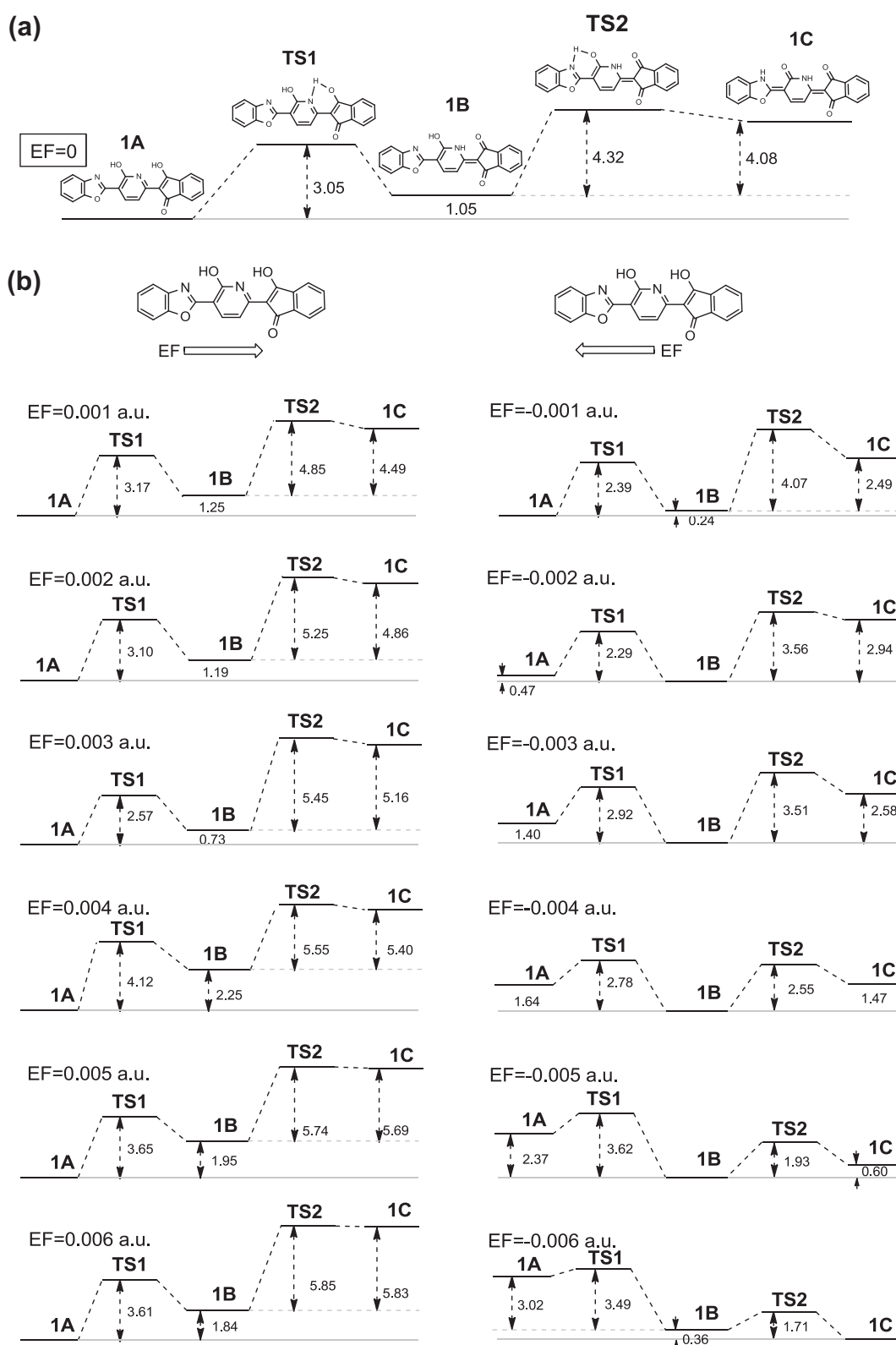


Fig. 6. Pathways between different tautomers of **1** without (a) and in presence (b) of applied electric field (EF). Relative energies (ΔG_{298}) and energy barriers (ΔG_{298}^\ddagger) are in kcal mol⁻¹.

the molecules and to an enhancement of the relative stability of **1A**. In negative EFs a reordering of the relative stabilities of the tautomers is observed as **1C** becomes the most stable structure

at EF = -0.006 and **1A** is about 3 kcal mol⁻¹ higher in energy. Thus, EF strength and polarity can lead to stabilization of different tautomeric forms.

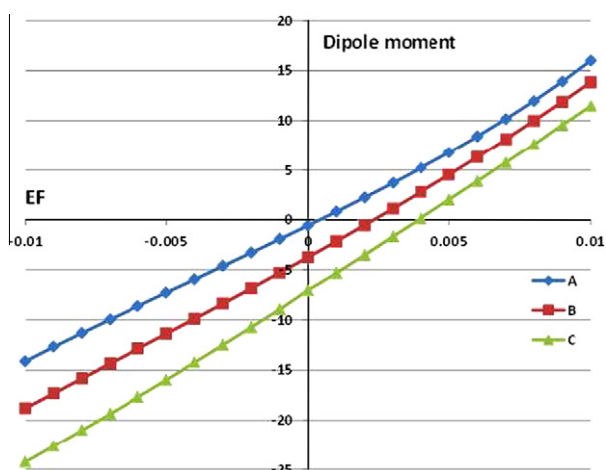


Fig. 7. Dipole moment component μ_x (Debye) as a function of the external EF (a.u.) for the three tautomers of **1**.

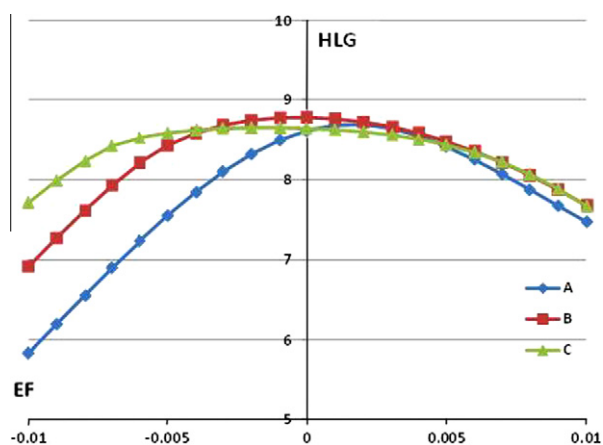


Fig. 8. HOMO–LUMO gap (eV) as a function of the external EF (a.u.) for the tautomers of **1**.

The prediction of the most stable structure for a given magnitude and polarity of the external field is feasible on the basis of the knowledge of the dependence of the induced dipole moments of a molecule, since the larger the induced dipole moment, the larger the stabilization in the external EF. The stabilization of **1A** in positive fields and **1C** in negative fields (Fig. 6) is further confirmed when considering the EF effect on the induced dipole moments. As the magnitude of the field increases (Fig. 7) the calculated induced dipole moments of **1A** in positive fields remain the largest whereas in negative fields **1C** has the largest negative dipole moment. It can be seen that the induced dipole moments increase in magnitude with the fields in a linear manner. The slopes of these (quasi)linear dependencies directly correspond to the molecular polarizabilities (the polarizability is the derivative of the dipole moment with respect to the applied field). The most moderate slope of **1A** and the steepest of **1C** correlate with the calculated longitudinal polarizabilities α_{xx} at MP2/6-31G(d,p) level: 547.7 a.u., 601.9 a.u. and 669.7 a.u. for **1A**, **1B** and **1C**, respectively. At fields higher than 0.005 a.u., the induced dipole moments deviate from linearity (especially for **1A**) and approximate a quadratic dependence on the applied external field.

Another electronic property that changes in an external electric field is the HOMO–LUMO gap (HLG). The decrease of the HLG (Fig. 8) is related to the polarization effect of the EF and is not monotonic as a function of the field strength. **1C** is characterized by a nearly symmetrical dependence on EF polarity whereas **1A** is more EF polarity dependent. When going from EF = 0.0 to EF = −0.01 the HLG of **1A** decreases by about 3 eV while for **1C** this decrease is less than 1 eV.

The spatial distribution of molecular orbitals allows to assess the electron transport properties of a molecular system [39,40]. A closer look at the frontier orbitals reveals a spatial redistribution of the HOMO and LUMO in the presence of an external EF. Fig. 9 displays the HOMO and LUMO plots at two electric field strengths, 0.006 a.u. and 0.01 a.u., and at both EF polarities as well as at zero EF for comparison. The spatial distribution at zero EF of the HOMO is very similar for the three tautomers with this orbital delocalized along the backbone of the molecules. The main difference may be observed in the LUMO orbital: in **1A** it is localized mainly on the **Hp** and **Ind** fragments, whereas in **1B** and **1C** it is quite delocalized.

With increase of the electric field, HOMOs and LUMOs shift in opposite directions from a delocalized to a partially localized state. In positive external electric fields, HOMOs move towards the higher potential and become more localized on fragments **Bo** and **Hp**; LUMOs move towards the lower potential, localizing predominantly on the **Ind** fragment, and this separation enhances with the field strength. This redistribution is more evident for LUMOs at EF = 0.01 a.u. In negative EFs, HOMOs and LUMOs are localized again in the opposite parts of the molecule but to a lesser extent – HOMO is spread over **Hp** and **Ind** whereas LUMO is on **Bo** and **Hp**. As seen from Fig. 9 at EF = −0.01 a.u. the LUMO of tautomer **1A**, in contrast to LUMO's of **1B** and **1C** has a small tail over the **Ind** moiety. Thus, in **1A** a larger delocalization over the molecular backbone is observed, which, in turn, leads to a LUMO stabilization and a smaller HLG with the EF increase.

This different behavior with respect to the EF polarity is due to the asymmetry of the molecules and their different polarizability. On the other hand, the differences in HLG and spatial distribution of the frontier orbitals of the three tautomers suggest that these compounds could act differently in view of their potential molecular device applications [41].

The effect of EF on molecular vibrations is revealed by changes in the frequencies and intensities of vibrational transitions [42]. The influence of EF on intensities can be explained by the appearance of an induced dipole moment as a result of EF polarization of the target molecule that leads to an alteration of the absolute value and direction of the corresponding vibrational transition dipole moments [42,43]. As it is known, the latter are related to the derivatives of the molecular electric dipole moments and/or polarizabilities with respect to the molecular vibrational coordinates. On the other hand, the applied external EF distorts the molecular force field (the position of potential energy minimum is displaced from the original one) and, as a result a frequency shift and/or splitting of degenerate modes can be observed [42–44]. In our theoretical study the EF effect is accompanied by electrostatic vibrational coupling between different frequency modes like C=O, NH and OH which take place in the proton transfer reaction. We studied their behavior with the increase of EF along the x-axis in the region (−0.006; −0.001 a.u.) where the tautomeric conversion is most probably expected (Fig. 6).

In general, a frequency decrease is observed for the stretching modes of C=O, NH and OH of the studied molecules with an increase of EF which can be explained by the above-mentioned displacement of potential energy minimum. At EF −0.006 a.u., tautomer **1C** becomes most stable, which is accompanied by a vibrational coupling between different C=O modes as well as between NH stretching modes. A similar picture is observed for NH


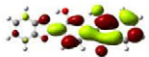



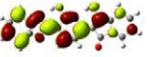

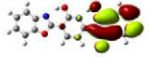





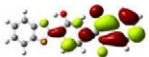



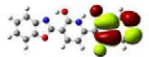












Tautomer	HOMO (E=0 a.u.)	LUMO (E=0 a.u.)		
A				
	HOMO (E=0.006 a.u.)	LUMO (E=0.006 a.u.)	HOMO (E=-0.006 a.u.)	LUMO (E=-0.006 a.u.)
				
	HOMO (E=0.010 a.u.)	LUMO (E=0.010 a.u.)	HOMO (E=-0.010 a.u.)	LUMO (E=-0.010 a.u.)
				
B	HOMO (E=0.0 a.u.)	LUMO (E=0.0 a.u.)		
				
	HOMO (E=0.006 a.u.)	LUMO (E=0.006 a.u.)	HOMO (E=-0.006 a.u.)	LUMO (E=-0.006 a.u.)
				
	HOMO (E=0.010 a.u.)	LUMO (E=0.010 a.u.)	HOMO (E=-0.010 a.u.)	LUMO (E=-0.010 a.u.)
				
C	HOMO (E=0.0 a.u.)	LUMO (E=0.0 a.u.)		
				
	HOMO (E=0.006 a.u.)	LUMO (E=0.006 a.u.)	HOMO (E=-0.006 a.u.)	LUMO (E=-0.006 a.u.)
				
	HOMO (E=0.010 a.u.)	LUMO (E=0.010 a.u.)	HOMO (E=-0.010 a.u.)	LUMO (E=-0.010 a.u.)
				

Fig. 9. Visualization of the frontier molecular orbitals of the three tautomers of **1** at different values (a.u.) of EF.

and OH stretching modes at $EF = -0.002$ a.u., where tautomer **1B** is predicted to be the most stable. However, such vibrational coupling is not observed for tautomer **1A** in the whole region of EF values (0.016, -0.016 a.u.). The predicted vibrational coupling effects could indicate tautomeric conversion between **1A** and **1B**, and **1B** and **1C**, on variation of the magnitude and direction of the applied external EF.

It is helpful to analyze the changes provoked by an external EF in the atomic charge distribution of a molecule. Since the IR intensities are directly related to the GAPT charges [28], these charges and their dependence on the EF could be informative for the charge fluxes and dipole moment variations induced by intramolecular charge transfer occurring during a vibration [45,46].

With an increase of the EF, the most significant deviations in the GAPT charges are observed for the atoms of fragment **Hp** and much smaller deviations are observed for the heteroatoms of the N–H and C=O bonds of the **Bo** and **Ind** fragments (Fig. 10). For the rest of the atoms, the calculated GAPT charges are almost independent of the EF strength and polarity. This shows that EF influences

mainly the electronic structure of the hydroxypyridine ring, where the EF could give rise to keto–enol conversion.

4. Concluding remarks

We propose and theoretically study a model system with small energy differences for its tautomeric forms and comparatively low activation barriers between them. Tautomers **1A–1C** are UV–vis distinguishable: the predicted longest wavelength absorption band of the most stable tautomer **1A** is at 462 nm, and **1B** and **1C** are hypsochromically shifted by 48 nm and 58 nm. The ab initio calculations with MP2 correlated method for the EF effect on the parent compound ($n = 1$) indicate that depending on the EF strength and polarity different tautomeric forms are stabilized. The external EF leads to a change of the electronic structures, such as reducing the HOMO–LUMO gap and the spatial redistribution of the frontier molecular orbitals. The distinct tautomeric structures are differently affected by the magnitude and direction of the applied EF.

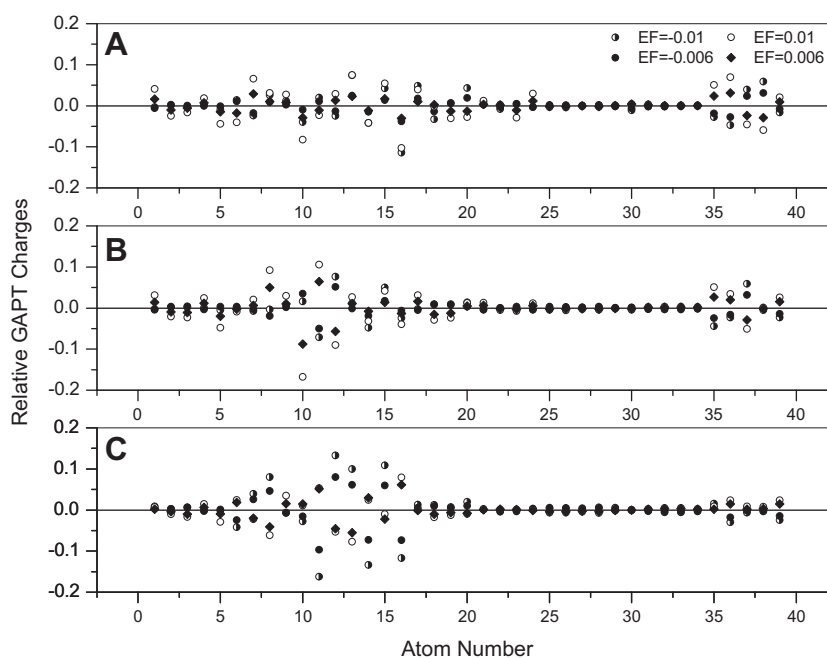


Fig. 10. Differences of atomic GAPT charges (e^-) of compound **1** relative to $EF = 0.0$ (a.u.) calculated at $EF = -0.01, -0.006, 0.006$ and 0.01 a.u. Atom numbers are given in Fig. 2.

Thus, the molecular responses can be tuned by applying suitable EF parameters. Due to the predicted asymmetry in HLG decrease upon EF direction the proposed model systems can be used in the design of molecular electronic devices such as molecular diodes, transistors, rectifiers and switches.

Acknowledgement

We acknowledge the financial support by the Bulgarian Fund for Scientific Research under Grant DO 02-217/2008.

Appendix A. Supplementary material

Supplementary data associated with this article can be found, in the online version, at <http://dx.doi.org/10.1016/j.comptc.2012.11.021>.

References

- [1] A. Aviram, M.A. Ratner, Molecular rectifiers, *Chem. Phys. Lett.* 29 (1974) 277–283.
- [2] L.A. Bumm, J.J. Arnold, M.T. Cygan, T.D. Dunbar, T.P. Burgin, L. Jones, D.L. Allara, J.M. Tour, P.S. Weiss, Are single molecular wires conducting?, *Science* 271 (1996) 1705–1707.
- [3] S. Jalili, H. Rafii-Tabar, Electronic conductance through organic nanowires, *Phys. Rev. B* 71 (2005) 165410–165418.
- [4] J.M. Tour, Molecular electronics synthesis and testing of components, *Accounts Chem. Res.* 33 (2000) 791–804.
- [5] R.M. Metzger, Unimolecular electrical rectifiers, *Chem. Rev.* 103 (2003) 3803–3834.
- [6] I.I. Oleynik, M.A. Kozhushner, V.S. Posvyanskii, L. Yu, Rectification mechanism in diblock oligomer molecular diodes, *Phys. Rev. Lett.* 96 (2006) 096803(1–4).
- [7] C. Joachim, J.K. Gimzewski, A. Aviram, Electronics using hybrid-molecular and mono-molecular devices, *Nature* 408 (2000) 541–548.
- [8] Z. Liu, A.A. Yasseri, J.S. Lindsey, D.F. Bocian, Molecular memories that survive silicon device processing and real-world operation, *Science* 302 (2003) 1543–1545.
- [9] R. McCreery, J. Dieringer, A.O. Solak, B. Snyder, A.M. Nowak, W.R. McGovern, S. DuVall, Molecular rectification and conductance switching in carbon-based molecular junctions by structural rearrangement accompanying electron injection, *J. Am. Chem. Soc.* 125 (2003) 10748–10758.
- [10] F. Chen, J. He, C. Nuckolls, T. Roberts, J.E. Klare, S. Lindsay, A molecular switch based on potential-induced changes of oxidation state, *Nano Lett.* 5 (2005) 503–506.
- [11] S. Yasuda, T. Nakamura, M. Matsumoto, H. Shigekawa, Phase switching of a single isomeric molecule and associated characteristic rectification, *J. Am. Chem. Soc.* 125 (2003) 16430–16433.
- [12] V. Luxami, S. Kumar, Molecular half-subtractor based on 3,3'-bis(1H-benzimidazolyl-2-yl)[1,1'-binaphthalenyl-2,2'-diol, *New J. Chem.* 32 (2008) 2074–2079.
- [13] F. D'Amore, M. Lanata, M.C. Gallazzi, G. Zerbi, Optical properties of a quinoid molecule, *Chem. Phys. Lett.* 377 (2003) 243–248.
- [14] R. Delgado, V. Hernandez, J. Casado, J.T. López Navarrete, J.M. Raimundo, P. Blanchard, J. Roncali, Vibrational study of push-pull chromophores for second-order non-linear optics derived from rigidified thiophene pi-conjugating spacers, *J. Mol. Struct.* 651 (2003) 151–158.
- [15] Z. Bayat, S. Danesh Nia, S.J. Mahdizadeh, Design of nanoscale molecular wire based on 3,6-diphenyl-1,2,4,5-tetrazine and effect of external electric field on electron transfer in conjugated molecular wire, *Physica E* 43 (2011) 1569–1575.
- [16] A. Mohajeri, A. Zare, Design of nanoscale molecular wire based on diphenylacetylene: role of linkage, *Comput. Mater. Sci.* 45 (2009) 935–940.
- [17] M. Karahka, H.J. Kreuzer, Conduction and electrostriction of polymers induced by high electric fields, *Polymers* 3 (2011) 51–64.
- [18] Z. Zhang, W. Guo, Energy-gap modulation of BN ribbons by transverse electric fields: first-principles calculations, *Phys. Rev. B* 77 (2008) 075403.
- [19] K. Selvaraju, M. Jothi, P. Kumaradhas, Understanding the charge density distribution and the electrostatic properties of hexadecane molecular nanowire under electric field using DFT and AIM theory, *Comput. Theoret. Chem.* 992 (2012) 9–17.
- [20] Y. Li, J. Zhao, X. Yin, H. Liu, G. Yin, Conformational analysis of diphenylacetylene under the influence of an external electric field, *Phys. Chem. Chem. Phys.* 9 (2007) 1186–1193.
- [21] Y.C. Choi, C. Pak, K.S. Kim, Electric field effects on water clusters ($n = 3–5$): systematic ab initio study of structures, energetics, and transition states, *J. Chem. Phys.* 124 (2006) 094308–094308–4.
- [22] S. Hammes-Schiffer, A.A. Stuchebrukhov, Theory of coupled electron and proton transfer reactions, *Chem. Rev.* 110 (2010) 6939–6960.
- [23] A.-R. Min, S.-J. Lee, M.-Y. Choi, R.E. Miller, Electric field dependence experiments and ab initio calculations of three cytosine tautomers in superfluid helium nanodroplets, *Bull. Korean Chem. Soc.* 30 (2009) 3039–3044.
- [24] V. Oklejas, R.H. Uibel, R. Horton, J.M. Harris, Electric-field control of the tautomerization and metal ion binding reactivity of 8-hydroxyquinoline immobilized to an electrode surface, *Anal. Chem.* 80 (2008) 1891–1901.
- [25] A.S. Klymchenko, A.P. Demchenko, Electrochromic modulation of excited-state intramolecular proton transfer: the new principle in design of fluorescence sensors, *J. Am. Chem. Soc.* 124 (2002) 12372–12379.
- [26] A.A. Granovsky, FIREFLY Quantum Chemistry Package, version 7.1.H, 2010, <<http://www.classic.chem.msu.su/gran/firefly/index.html>>.
- [27] Y.W. Li, Y. Zhang, G.P. Yin, J.W. Zhao, Theoretical investigations on molecular conducting wire under electric field, *Chem. J. Chin. Univ. – Chin.* 27 (2006) 292–296.

- [28] J. Cioslowski, A new population analysis based on atomic polar tensors, *J. Am. Chem. Soc.* 111 (1989) 8333–8336.
- [29] D. Sundholm, Density functional theory calculations of the visible spectrum of chlorophyll a, *Chem. Phys. Lett.* 302 (1999) 480–484.
- [30] A. Masunov, S. Tretiak, Prediction of two-photon absorption properties for organic chromophores using time-dependent density-functional theory, *J. Chem. Phys. B* 108 (2004) 899–907.
- [31] F.C. Grozema, P.T. van Duijnen, L.D.A. Siebbeles, A. Goossens, S.W. de Leeuw, Electronic structure of thienylene vinylene oligomers: singlet excited states, triplet excited states, cations, and dications, *J. Phys. Chem. B* 108 (2004) 16139–16146.
- [32] D. Rappoport, F. Furche, Photoinduced intramolecular charge transfer in 4-(dimethyl)aminobenzonitrile – a theoretical perspective, *J. Am. Chem. Soc.* 126 (2004) 1277–1284.
- [33] M. Guillaume, B. Champagne, F. Zutterman, Investigation of the UV/visible absorption spectra of merocyanine dyes using time-dependent density functional theory, *J. Phys. Chem. A* 110 (2006) 13007–13013.
- [34] C. Adamo, V. Barone, Accurate excitation energies from time-dependent density functional theory: assessing the PBE0 model for organic free radicals, *Chem. Phys. Lett.* 314 (1999) 152–157.
- [35] C. Adamo, V. Barone, Toward reliable density functional methods without adjustable parameters: the PBE0 model, *J. Chem. Phys.* 110 (1999) 6158–6170.
- [36] Y.L. Li, L. Han, Y. Mei, J.Z.H. Zhang, Time-dependent density functional theory study of absorption spectra of metallocenes, *Chem. Phys. Lett.* 482 (2009) 217–222.
- [37] D. Jacquemin, E.A. Perpète, G. Scalmani, I. Ciofini, C. Peltier, C. Adamo, Absorption and emission spectra of 1,8-naphthalimide fluorophores: A PCM-TD-DFT investigation, *Chem. Phys.* 372 (2010) 61–66.
- [38] M.J. Frisch, G.W. Trucks, H.B. Schlegel, G.E. Scuseria, M.A. Robb, G. Scalmani, V. Barone, B. Mennucci, G.A. Petersson, H. Nakatsuji, M. Caricato, X. Li, H.P. Hratchian, A.F. Izmaylov, J. Bloino, G. Zheng, J.L. Sonnenberg, M. Hada, M. Ehara, K. Toyota, et al., Gaussian 09 Revision A01, Gaussian Inc., Wallingford CT, 2009.
- [39] J. Heurich, J.C. Cuevas, W. Wenzel, G. Schön, Electrical transport through single-molecule junctions: from molecular orbitals to conduction channels, *Phys. Rev. Lett.* 88 (2002) 256803.
- [40] V. Mujica, A. Nitzan, S. Datta, M.A. Ratner, C.P. Kubiak, Molecular wire junctions: tuning the conductance, *J. Phys. Chem. B* 107 (2003) 91–95.
- [41] J.L. Rao, Qualitative and quantitative analysis of electron transport in donor/acceptor-heterocycles connected to cumulenyl bridge, *Acta Chim. Slov.* 56 (2009) 826–834.
- [42] G. Maroulis, *Atoms Molecules and Clusters in Electric Fields Theoretical Approaches to the Calculation of Electric Polarizability*, Imperial College Press, 2006.
- [43] E.S. Park, S.G. Boxer, Origins of the sensitivity of molecular vibrations to electric fields: carbonyl and nitrosyl stretches in model compounds and proteins, *J. Phys. Chem. B* 106 (2002) 5800–5806.
- [44] R. Kahn, E.C. De Lara, K.D. Möller, Effect of an electric field on a methane molecule II calculation of the degeneracy splitting of the ν_3 band expression of the second derivatives of the CH_4 dipole moment and evaluation of the second derivative of the C–H bond polarizability, *J. Chem. Phys.* 83 (1985) 2653–2660.
- [45] R.L.A. Haiduke, R.E. Bruns, An atomic charge-charge flux-dipole flux atom-in-molecule decomposition for molecular dipole-moment derivatives and infrared fundamental intensities, *J. Phys. Chem. A* 109 (2005) 2680–2688.
- [46] T.C.F. Gomes, J.V. da Silva, L.N. Vidal, P.A.M. Vazquez, R.E. Bruns, ChelpG and QTAIM atomic charge and dipole models for the infrared fundamental intensities of the fluorochloromethanes, *Theor. Chem. Acc.* 121 (2008) 173–179.